$K^*(892)^+$ production in proton-proton collisions at $E_{\text{beam}} = 3.5$ GeV

G. Agakishiev,[7] O. Arnold,[10,9] D. Belver,[18] A. Belyaev,[7] J. C. Berger-Chen,[10,9] A. Blanco,[2] M. Böhmer,[10] J. L. Boyard,[16] P. Cabanelas,[18] S. Chernenko,[7] A. Dybczak,[3] E. Epple,[10,9] L. Fabbietti,[10,9] O. Fateev,[7] P. Finocchiaro,[1] P. Fonte,[2,20] J. Friese,[10] I. Fröhlich,[8] T. Galatyuk,[5,21] J. A. Garzón,[18] R. Gernhäuser,[10] K. Göbel,[8] M. Golubeva,[13] M. González-Díaz,[5] F. Guber,[13] M. Gumberidze,[5,21] T. Heinz,[4] T. Hennino,[16] R. Holzmann,[4] A. Ierusalimov,[7] I. Iori,[12,23] A. Ivashkin,[13] M. Jurkovic,[10] B. Kämpfer,[6,22] T. Karavicheva,[13] I. Koenig,[4] W. Koenig,[4] B. W. Kolb,[4] G. Korcyl,[3] G. Kornakov,[5] R. Kotte,[6] A. Krása,[17] F. Krizek,[17] R. Krücken,[10] H. Kuc,[3,16] W. Kühn,[11] A. Kugler,[17] T. Kunz,[10] A. Kurepin,[13] V. Ladygin,[7] R. Lalik,[10,9] K. Lapidus,[10,9,*] A. Lebedev,[14] L. Lopes,[2] M. Lorenz,[8,26] L. Maier,[10] A. Mangiarotti,[2] J. Markert,[8] V. Metag,[11] J. Michel,[8] D. Mihaylov,[10,9,†] C. Müntz,[8] R. Münzer,[10,9] L. Naumann,[6] Y. C. Pachmayer,[8] M. Palka,[3] Y. Parpottas,[15,24] V. Pechenov,[4] O. Pechenova,[8] J. Pietraszko,[4] W. Przygoda,[3] B. Ramstein,[16] A. Reshetin,[13] A. Rustamov,[8] A. Sadovsky,[13] P. Salabura,[3] A. Schmah,[19] E. Schwab,[4] J. Siebenson,[10,9] Yu. G. Sobolev,[17] S. Spataro,[25] B. Spruck,[11] H. Ströbele,[8] J. Stroth,[8,4] C. Sturm,[4] O. Svoboda,[17] A. Tarantola,[8] K. Teilab,[8] P. Tlusty,[17] M. Traxler,[4] H. Tsertos,[15] T. Vasiliev,[7] V. Wagner,[17] M. Weber,[10] C. Wendisch,[4] J. Wüstenfeld,[6] S. Yurevich,[4] and Y. Zanevsky[7]

(HADES Collaboration)

[1]*Istituto Nazionale di Fisica Nucleare - Laboratori Nazionali del Sud, 95125 Catania, Italy*
[2]*LIP-Laboratório de Instrumentação e Física Experimental de Partículas, 3004-516 Coimbra, Portugal*
[3]*Smoluchowski Institute of Physics, Jagiellonian University of Cracow, 30-059 Kraków, Poland*
[4]*GSI Helmholtzzentrum für Schwerionenforschung GmbH, 64291 Darmstadt, Germany*
[5]*Technische Universität Darmstadt, 64289 Darmstadt, Germany*
[6]*Institut für Strahlenphysik, Helmholtz-Zentrum Dresden-Rossendorf, 01314 Dresden, Germany*
[7]*Joint Institute of Nuclear Research, 141980 Dubna, Russia*
[8]*Institut für Kernphysik, Goethe-Universität, 60438 Frankfurt, Germany*
[9]*Excellence Cluster 'Origin and Structure of the Universe', 85748 Garching, Germany*
[10]*Physik Department E12, Technische Universität München, 85748 Garching, Germany*
[11]*II.Physikalisches Institut, Justus Liebig Universität Giessen, 35392 Giessen, Germany*
[12]*Istituto Nazionale di Fisica Nucleare, Sezione di Milano, 20133 Milano, Italy*
[13]*Institute for Nuclear Research, Russian Academy of Science, 117312 Moscow, Russia*
[14]*Institute of Theoretical and Experimental Physics, 117218 Moscow, Russia*
[15]*Department of Physics, University of Cyprus, 1678 Nicosia, Cyprus*
[16]*Institut de Physique Nucléaire (UMR 8608), CNRS/IN2P3 - Université Paris Sud, F-91406 Orsay Cedex, France*
[17]*Nuclear Physics Institute, Academy of Sciences of Czech Republic, 25068 Rez, Czech Republic*
[18]*LabCAF. F. Física, Univ. de Santiago de Compostela, 15706 Santiago de Compostela, Spain*
[19]*Lawrence Berkeley National Laboratory, Berkeley, USA*
[20]*ISEC Coimbra, Coimbra, Portugal*
[21]*ExtreMe Matter Institute EMMI, 64291 Darmstadt, Germany*
[22]*Technische Universität Dresden, 01062 Dresden, Germany*
[23]*Dipartimento di Fisica, Università di Milano, 20133 Milano, Italy*
[24]*Frederick University, 1036 Nicosia, Cyprus*
[25]*Dipartimento di Fisica and INFN, Università di Torino, 10125 Torino, Italy*
[26]*Utrecht University, 3584 CC Utrecht, The Netherlands*

We present results on the $K^*(892)^+$ production in proton-proton collisions at a beam energy of $E = 3.5$ GeV, which is hitherto the lowest energy at which this mesonic resonance has been observed in nucleon-nucleon reactions. The data are interpreted within a two-channel model that includes the three-body production of $K^*(892)^+$ associated with the Λ or Σ hyperon. The relative contributions of both channels are estimated. Besides the total cross section $\sigma(p + p \rightarrow K^*(892)^+ + X) = 9.5 \pm 0.9^{+1.1}_{-0.9} \pm 0.7$ μb, which adds a new data point to the excitation function of the $K^*(892)^+$ production in the region of low excess energy, transverse momenta and angular spectra are extracted and compared with the predictions of the two-channel model. The spin characteristics of $K^*(892)^+$ are discussed as well in terms of the spin-alignment.

PACS number(s): 25.40.Ve, 14.40.Df, 25.75.Dw

I. INTRODUCTION

*kirill.lapidus@ph.tum.de
†dimitar.mihaylov@mytum.de

The production of the strange vector meson $K^*(892)$ in proton-proton (pp) collisions was studied rather extensively at high collision energies [1–7], with the lowest-energy data

point at $\sqrt{s} = 4.93$ GeV [8]. No data, however, exist in the region close to the production threshold $\sqrt{s_{thr}} = 2.95$ GeV. This is in contrast to the situation with the kaon ground state, the production of which has been measured both inclusively and exclusively in a broad range of energies, including the very vicinity of its production threshold. The production of kaons and their excitations in proton-proton collisions is governed by the conservation of strangeness, so the simplest possible reaction reads

$$p + p \rightarrow N + Y + K/K^*(892), \qquad (1)$$
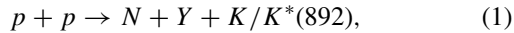
where N stands for the nucleon and Y for the ground-state hyperons $\Lambda(1116)$ or $\Sigma(1189)$. The three-body kaon production has been studied in detail at low excess energies [9,10], and it was established that, for energies close to the production threshold, the kaon production is mainly accompanied by a $\Lambda(1116)$-hyperon rather than a $\Sigma(1189)$. It is of interest, therefore, to identify the preferable formation mechanism of the K^* meson as well.

In this paper we discuss the study of the $K^*(892)^+$ production in proton-proton collisions performed by the HADES collaboration. The deep subthreshold K^* production was analyzed in Ref. [11] for Ar+KCl reactions at a beam energy of 1.756 GeV. In view of future experiments at the Facility for Antiproton and Heavy-Ion Research (FAIR) exploring heavy ion collisions at energies of 2–8 GeV/nucleon, new data from proton-proton reactions are essential as reference measurements and input for transport models. This work complements our previous studies of inclusive and exclusive strangeness production in proton-proton reactions at 3.5 GeV, namely K^0 [12], $\Sigma(1385)^+$ [13], $\Lambda(1405)$ [14,15], and $pK^+\Lambda$ [16]. The paper is organized as follows. Section II gives a brief information about the experimental setup. The particle selection and K^* reconstruction procedure is described in Sec. III. Section IV contains the obtained results, their interpretation within the two-channel model, and a discussion of the spin alignment measurement. The summary can be found in Sec. V.

II. THE EXPERIMENT

The experimental data stem from the High-Acceptance Di-Electron Spectrometer (HADES), installed at the SIS18 synchrotron (GSI Helmholtzzentrum, Darmstadt). The detector tracking system consists of a superconducting magnet and four planes of multiwire drift chambers (MDC). The particle identification capabilities are extended by the time-of-flight wall and a ring imaging Cherenkov (RICH) detector. The detector, as implied by its name, is characterized by a large acceptance both in the polar (from $18°$ to $85°$) and azimuthal angles. The detector subsystems are described in detail in Ref. [17]. In 2007 a measurement of proton-proton collisions at a kinetic beam energy of 3.5 GeV was performed: the beam with an average intensity of about 1×10^7 particles/s was incident on a liquid hydrogen target with an area density of 0.35 g/cm^2 corresponding to total interaction probability of $\sim 0.7\%$. In total, 1.2×10^9 events were collected. The first-level trigger (LVL1) required at least three hits in the time-of-flight wall in order to suppress elastic scattering events.
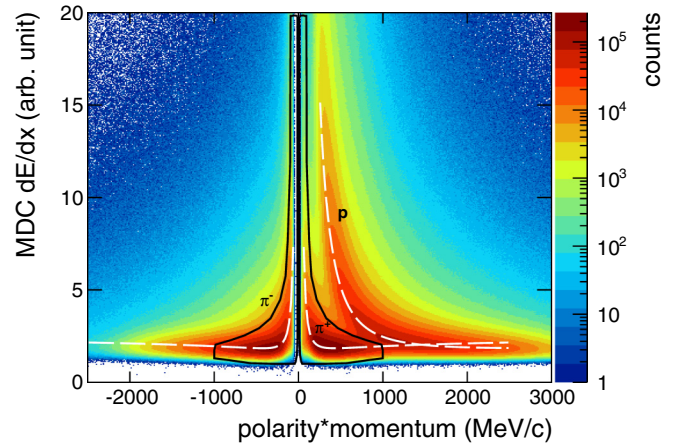

FIG. 1. (Color online) Specific energy loss of charged particles in MDC chambers as a function of the momentum times polarity. Solid curves show graphical cuts for the $\pi^\pm$ selection. The Bethe-Bloch curves are shown by dashed curves.

III. DATA ANALYSIS

A. K^* reconstruction

The $K^*(892)^+$ meson decays strongly, at the primary pp-reaction vertex, into a kaon-pion pair. The decay mode $K^*(892)^+ \rightarrow K^0\pi^+$ with a branching ratio of 2/3 is particularly suited for the analysis, since the short-lived component of the K^0, the K_S^0, decays weakly into a $\pi^+\pi^-$ pair ($c\tau = 2.68$ cm, branching ratio 69.2%). The considered final state of the $K^*(892)^+$ decay is, therefore, composed out of three charged pions, two of which are emitted from a secondary vertex. Therefore, as a first step of the analysis, we select events with (at least) three pions, identified by a selection on the $(dE/dx)_{MDC}$-momentum plane (Fig. 1). The variable $(dE/dx)_{MDC}$ is the cumulative specific energy loss of a charged particle in the four MDC planes.

In the next step we consider all triplets of charged pions ($\pi^+\pi^+\pi^-$) that were found in one event. Since two positively charged pions are available, two K_S^0-candidates are constructed for each triplet. Afterwards, to ensure that the K_S^0 decayed away from the primary vertex, and, thus, reduce the combinatorial background, a set of topological cuts was applied to the $\pi^+\pi^-$ pair that forms the K_S^0 candidate. These were: (i) a cut on the distance between the primary and the secondary vertex $d(K_S^0 - V) > 28$ mm, (ii) a cut on the distance of closest approach between two pion tracks, $d_{\pi^+-\pi^-} < 13$ mm, and (iii) a cut on the distance of closest approach between either of the extrapolated pion tracks and the primary vertex $DCA_\pi^{K^0} > 8$ mm. Besides, a cut on the distance of closest approach between the pion track *not associated* to the K_S^0 candidate (i.e., stemming from the K^* decay) and the primary vertex $DCA_\pi^{K^*} < 6$ mm, has been introduced. The application of the topological cuts reduces the double-counting probability (i.e., identifying more than one K_S^0 candidate in one event, which is kinematically forbidden at this collision energy) to 6%. The invariant mass spectrum of the $\pi^+\pi^-$ pairs that passed the topological cuts is shown in Fig. 2. A prominent K_S^0 signal is visible. In total, about 24×10^3 K_S^0
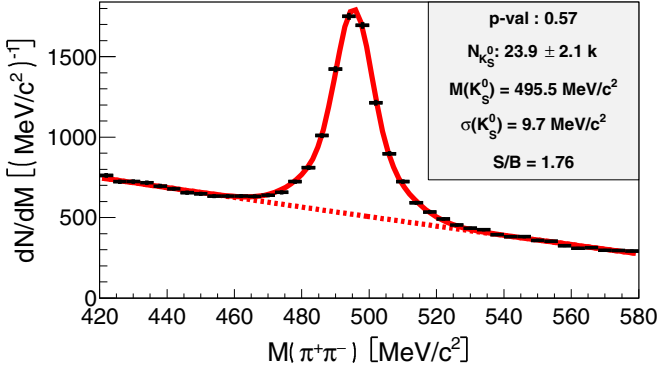
FIG. 2. (Color online) $\pi^+\pi^-$ invariant mass distribution from events with at least three pions used for the K_S^0 reconstruction. The legend delivers information on the fit p value, the number of K_S^0 over background, extracted mass, width, and signal to background ratio.

candidates were reconstructed in events with at least three charged pions.

In the next step we applied a cut on the invariant mass of the $\pi^+\pi^-$ pairs, i.e., a 19.4 MeV/c^2 interval ($\pm 1\sigma$) centered at the K_S^0 mass peak at 495.5 MeV/c^2 and combined the pairs passing the cut with the remaining positively charged pion. The resulting invariant mass distributions of the $K_S^0 - \pi^+$ system are shown in Fig. 3 for the total sample (upper left panel) and separately in five transverse momentum bins. A clear signal of the sought-after K^* is visible on top of

the combinatorial background that can be divided into two classes: (i) $\pi^+\pi^+\pi^-$ triplets produced in reactions without strangeness involvement, and (ii) nonresonant production of $K_S^0\pi^+$ pairs. The total statistics of about 1700 K^* allows for a one-dimensional differential analysis. Below we discuss the extraction of the transverse momentum spectra in detail; the procedure can be applied to any kinematical variable. The extraction of the raw (i.e., neither corrected for the limited geometrical acceptance of the HADES detector nor for the efficiency of the analysis procedure) K^* yields is carried out with fits of the experimental invariant mass distributions. After a careful study of the best way to approximate the experimental distributions, we used the following function:

$$f(M) = F_{\mathrm{PS}}(M) \times V(M;\Gamma,\sigma) + P_3(M), \qquad (2)$$

where M is the invariant mass of $K_S^0\pi^+$ pairs, $F_{\mathrm{PS}}(M)$—the factor that takes into account phase-space limitations, $V(M;\Gamma,\sigma)$—the Voigt function, and $P_3(M)$—a third degree polynomial that models the nonresonant background. The parameters of the Voigt function are: (i) Γ, internal width of K^* that was fixed to the PDG value of 50.8 MeV [18], and (ii) σ, the detector resolution (instrumental width) that was determined (and fixed as well) to be about 11 MeV by simulating a sample of zero-width K^*'s. The phase space distortion factor $F_{\mathrm{PS}}(M)$ depends on the production channel (Λ- or Σ-associated), so first we shall introduce the two-channel simulation model.
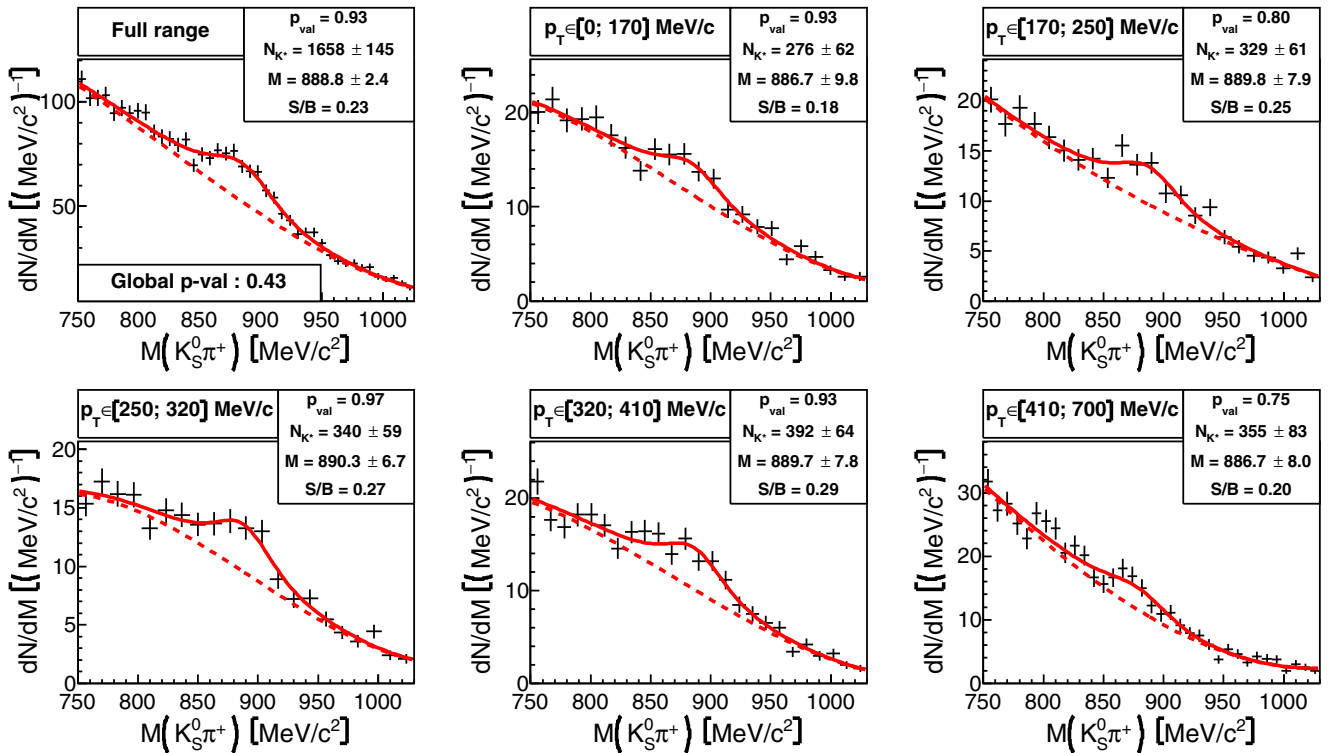

FIG. 3. (Color online) Invariant mass spectra of K_S^0-π^+ pairs (symbols) for the total sample (upper left) and in five transverse momentum bins. Solid curves are for the fits with 2, dashed curves depict the background, separately. The boxes deliver information on the fit p value, the number of K^* over background, mean mass, and signal-to-background ratio.

B. Two-channel model

Due to the quite low beam energy, the three following three-body channels are expected to dominate K^* production:

$$p + p \rightarrow p + \Lambda + K^*(892)^+, \tag{3}$$

$$p + p \rightarrow p + \Sigma^0 + K^*(892)^+, \tag{4}$$

$$p + p \rightarrow n + \Sigma^+ + K^*(892)^+. \tag{5}$$

Here we neglect the contribution of the four-body channels with an additional pion ($p + p \rightarrow N + \pi + Y + K^*$). They are energetically possible but are expected to be suppressed in comparison with the three-body channels. As it will be shown below, this assumption is confirmed by the experimental data. We make another simplification, namely we consider only one Σ-associated channel ($p\Sigma^0 K^*$) out of two that are allowed. Up to the small differences in the masses of the reaction products, both channels have exactly the same kinematics and are indistinguishable in the inclusive analysis of K^*. Hence, we employ hereafter a two-channel model that includes the Λ and the Σ channels, where the latter has to be understood as the sum of the two isospin-splitted subchannels. The invariant mass distributions of the simulated K^*'s were reconstructed for both channels of the model. Then, the phase-space factor $F_{PS}(M)$ was determined, which takes into account the deviation from an ideal Breit-Wigner shape. As the contributions of both channels are not known *a priori*, the phase-space factor is constructed as the sum of the two individual contributions from the Λ and Σ channel:

$$F_{PS}(M) = A_\Lambda \times F_{PS}^\Lambda(M) + A_\Sigma \times F_{PS}^\Sigma(M). \tag{6}$$

It was found that the fitting procedure is not sensitive to the exact contribution of each channel (i.e., to the weights A_Λ and A_Σ).

C. Raw spectra and corrections

Fits of the experimental data, performed with Eq. (2), allow us to extract the raw yields (affected by the finite acceptance of the detector and efficiency of the analysis procedure). As an example, the raw p_t spectrum of the K^* mesons is shown in Fig. 4. Also shown are K^* distributions
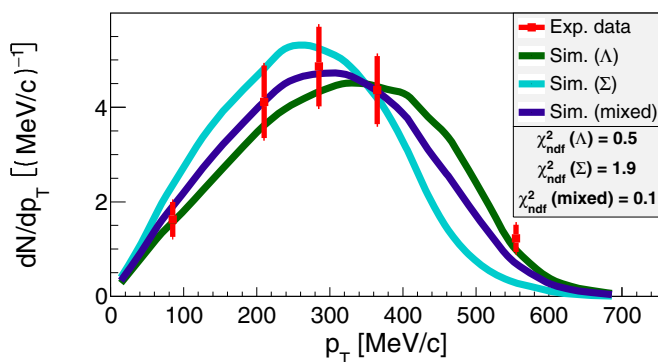
corresponding to the Λ and Σ channels of the two-channel model. They were obtained in the following way. A set of events (four-vectors of the reactions products) corresponding to both channel Eqs. (3) and (4) were simulated with the PLUTO Monte Carlo generator [19]. A uniform population of the three-body phase-space has been assumed: neither any kind of angular anisotropy has been implemented, nor any contribution from an N^*- or Δ-resonance coupling to the K^*-Y pair considered. Afterwards, these events served as input for the full-scale simulation procedure that includes the propagation of particles in the detector (the GEANT3 code was employed), track reconstruction, etc. Finally, the simulated data sample was analyzed in the same way as the experimental one. All simulated curves shown in Fig. 4 are normalized to the integral of the experimental distribution. Furthermore, an optimal mixture of the two channels has been determined by means of a χ^2 analysis, delivering the value for the relative Σ-channel contribution of 0.4 ± 0.2, where 0.2 is the dominating systematic uncertainty determined by the variation of the experimental cuts, as will be explained below. The resulting mixed spectrum is shown in Fig. 4 as well. A contribution of the four-body channels ($N\pi Y K^*$ final state) would produce an even softer p_t spectrum as compared to the one generated by the Σ channel and, therefore, is completely negligible in this analysis. Finally, we note that an analysis of the missing mass to the $K^* p$ final state, potentially more selective with respect to the Λ or Σ contributions, is not feasible due to the limited statistics.

As the constructed model ("$0.6 \times \Lambda + 0.4 \times \Sigma$") describes the data very well, we can use it to correct the raw experimental yields. Due to the limited statistics of the experimental data we perform a one-dimensional correction. The efficiency and acceptance depend, thus, on one kinematical variable. We exemplify the procedure for the p_t variable; all other variables are treated analogously.

For the purpose of the efficiency correction we prepare a histogram I, which corresponds to the p_t spectrum of the simulated K^*'s in the full solid angle, not affected by the limited geometrical acceptance of the detector and efficiency of the analysis procedure. A histogram O corresponds to

FIG. 4. (Color online) Raw p_t spectrum of K^*'s produced in proton-proton reactions. Markers—experimental data with statistical uncertainties, curves—expectations from the channel Eqs. (3), (4), and their mixture "$0.6 \times \Lambda + 0.4 \times \Sigma$."
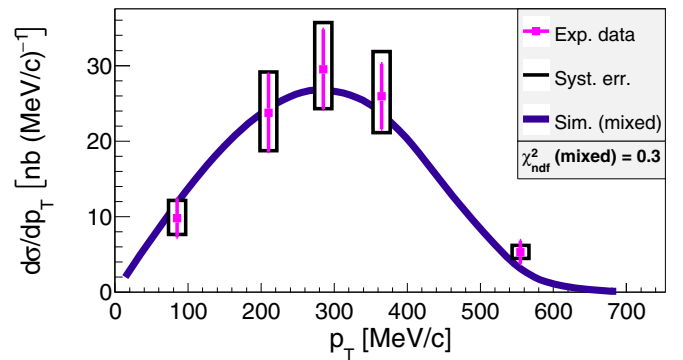

FIG. 5. (Color online) K^* transverse momentum spectrum. Markers—experimental data with statistical uncertainties, empty boxes—systematical uncertainties. The two-channel model ("$0.6 \times \Lambda + 0.4 \times \Sigma$") final-state phase-space distribution is shown by the solid curve.
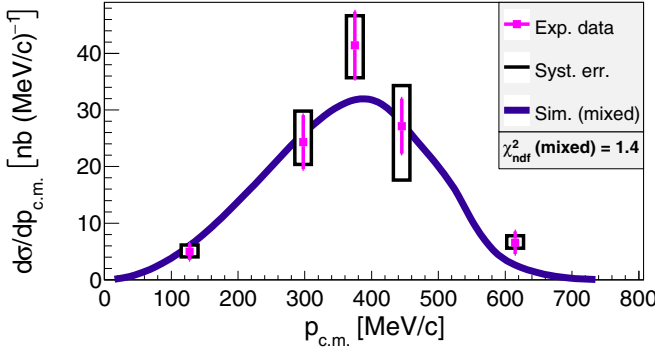
FIG. 6. (Color online) Same as described in the caption of Fig. 5 for the momentum spectrum in the pp center-of-mass reference frame.

the p_t spectrum of K^*'s that went through full simulation and analysis chain. Finally, the ratio $\epsilon(p_t) = O/I$ is the efficiency histogram. Dividing bin-wise the raw experimental p_t spectrum by the $\epsilon(p_t)$ histogram, we obtain the acceptance- and efficiency-corrected spectrum.

IV. RESULTS AND DISCUSSION

Figure 5 shows the acceptance and efficiency corrected p_t spectrum of K^*. The experimental data are normalized absolutely based on the analysis of the proton-proton elastic scattering channel in the HADES acceptance, as has been done for the inclusive dielectron analysis [20]. To no surprise (cf. Fig. 4), the corrected spectrum is very well described by the two-channel model that assumes a 40% contribution of the Σ channel.

As mentioned already, a one-dimensional analysis, exemplified above with the transverse momentum variable, can be performed for any chosen kinematical variable. For completeness, Figs. 6 and 7 show corrected spectra for the total momentum and angular distribution in the pp center-of-mass reference frame, respectively.

Remarkably, all three selected (p_t, $p_{c.m.}$, and $\cos\theta_{c.m.}$) projections of a three-dimensional single-particle phase space are well described by the two-channel model. No significant
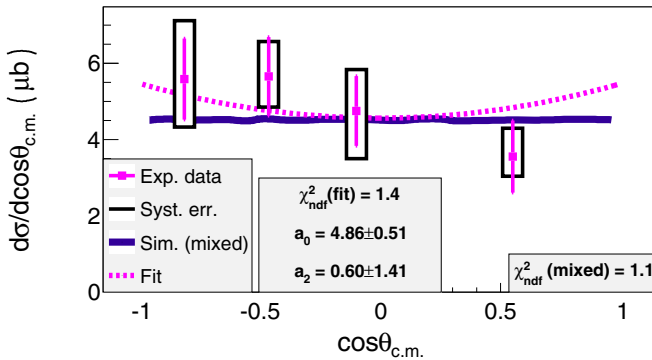

FIG. 7. (Color online) Same as described in the caption of Fig. 5 for the angular spectrum in the pp center-of-mass reference frame. The dashed curve correspond to the fit with Legendre polynomials (only 0th and 2nd order are used due to the symmetry arguments, resulting coefficients are shown in the inset).

TABLE I. Topological and the K_S^0 invariant mass cut variations used to estimate the systematic uncertainty. For all cut combinations the condition $DCA_\pi^{K^*} \leqslant DCA_\pi^{K^0}$ has been demanded, reducing 1800 cut combinations to 1200.

Observable	Lower value	Upper value	Steps
$d(K_S^0 - V)$ [mm]	>24	>40	5
$d_{\pi^+-\pi^-}$ [mm]	<7	<13	4
$DCA_\pi^{K^0}$ [mm]	>5.6	>16	5
$DCA_\pi^{K^*}$ [mm]	<3	<16	6
$\Delta M_{K_S^0}$ [MeV/c^2]	9.7(1σ)	19.4(2σ)	3

angular anisotropy is observed for the K^* emission in proton-proton collisions: a Legendre-polynomial fit (dotted curve in Fig. 7) does not deliver a better χ^2 as compared to the isotropic (by construction) distribution of the two-channel model. The integration of the experimental p_t-spectrum (Fig. 5) allows us to extract the total cross-section of the inclusive K^{*+} production:

$$\sigma[p + p \to K^*(892)^+ + X] = 9.5 \pm 0.9^{+1.1}_{-0.9} \pm 0.7\,\mu b, \quad (7)$$

where the statistical (first), systematic (second), and normalization (third) uncertainties are given. The systematic uncertainty was estimated by a variation of the experimental cuts (topological cuts plus K_S^0 selection via an invariant mass constraint). The values of the cuts used for this variation are listed in Table I. In total, 1200 cut combinations have been tested. For each cut combination new invariant mass fits were performed along with new efficiency corrections. Afterwards, from the distribution of the total cross-section a central interval covering 68% of the outcomes has been identified. The borders of this interval—asymmetric with
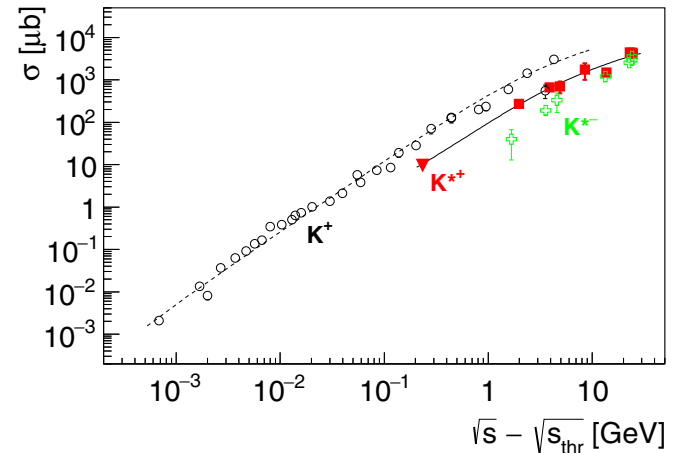

FIG. 8. (Color online) Energy ($\sqrt{s} - \sqrt{s_{thr}}$) dependence of the total cross-section for the processes: (i) pp $\to K^*(892)^+X$ (red squares, world data [1,2,4–8]; red triangle, present work), (ii) pp $\to K^*(892)^-X$ (empty green crosses) [2,4–8], and (iii) pp $\to K^+X$ (empty circles) ([9,10,21] and references therein). The solid (dashed) line is a fit to the $K^*(892)^+$ (K^+) data with $f(x) = C[(1 - (D/x)^\mu]^\nu$, where $x = \sqrt{s}$. The numerical values are $C = 3.22 \times 10^6 (1.04 \times 10^5)$, $D = 2.89(2.55)$ GeV, $\mu = 1.19 \times 10^{-2}(1.16 \times 10^{-1})$, $\nu = 1.86(1.67)$.
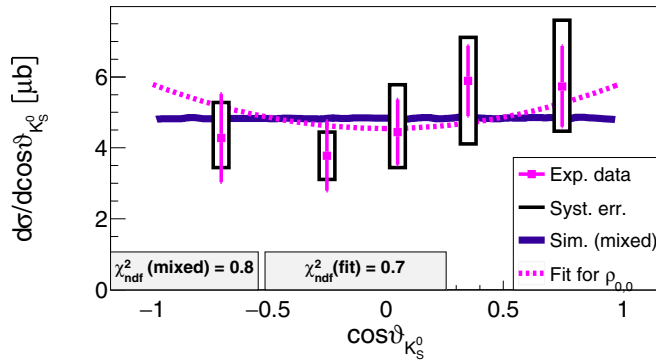
FIG. 9. (Color online) Angular distribution of K_S^0 in the K^* rest frame. Markers, experimental data with statistical uncertainties; empty boxes, systematical uncertainties. The two-channel model ("$0.6 \times \Lambda + 0.4 \times \Sigma$") final-state phase-space distribution as simulated with PLUTO without any spin alignment is shown by the solid curve. The dashed curve is the fit of Eq. (8) to the data with $\rho_{00} = 0.39$.

respect to the median value—define the systematic uncertainty quoted in Eq. (7).

The extracted total cross-section value complements the K^* excitation function shown in Fig. 8 in the low-energy region, where measurements were not available until now. The HADES data point is consistent with the trend set by the measurements at higher energies.

In comparison to the ground state, the K^* carries spin one, so we proceed with the discussion of its polarization properties as probed in proton-proton collisions. The spin configuration of the K^* in the final state is described by the spin density matrix $\rho_{mm'}$. The diagonal elements ρ_{11}, ρ_{00}, and ρ_{1-1} define, respectively, the probabilities of the $+1$, 0, and -1 spin projections on the quantization axis. The ρ_{00} can be extracted from the angular distribution of the decay products (K^0 or π^+) in the rest frame of K^* [22] via

$$W(\vartheta) = \tfrac{3}{4}[(1 - \rho_{00}) + (3\rho_{00} - 1)\cos^2(\vartheta)]. \qquad (8)$$

The situation with $\rho_{00} \neq 1/3$ is referred to as the *spin-alignment* case, i.e., not equally probable populations of the ± 1 and 0 spin projections. The angular distribution of interest

is shown in Fig. 9. Our fit with Eq. (8) gives the following result:

$$\rho_{00} = 0.39 \pm 0.09(\text{stat.})^{+0.10}_{-0.09}(\text{syst.}). \qquad (9)$$

Within uncertainties our measurement is fully consistent with $\rho_{00} = 1/3$; i.e., no spin-alignment of K^* is observed.

V. SUMMARY AND CONCLUSIONS

To summarize, we presented here the hitherto lowest-energy measurement of the $K^*(892)^+$ production in proton-proton collisions. The relative contribution of the channel $p + p \rightarrow p + \Sigma + K^*(892)^+$ has been estimated as 0.4 ± 0.2. Within uncertainties of the experimental data, no deviations from a three-body phase-space population have been identified in the kinematical distributions of K^*, as well as no convincing signal of a spin-alignment has been observed.

This measurement sets a baseline for future studies of K^* production in proton-nucleus and heavy-ion collisions. For instance, by comparing the present data with previously measured by HADES proton-niobium collisions at the same beam energy, cold nuclear matter effects affecting the production of the K^*'s can be extracted.

[1] V. Ammosov *et al.* (French-Soviet Collaboration), SACLAY-DPhPE 75-08, IFVE-M-19 (1975).

[2] H. Kichimi *et al.*, Lett. Nuovo Cim. **24**, 129 (1979).

[3] D. Drijard *et al.* (Annecy-CERN-Collège de France-Dortmund-Heidelberg-Warsaw Collaboration), Z. Phys. C **9**, 293 (1981).

[4] D. Brick *et al.*, Phys. Rev. D **25**, 2248 (1982).

[5] T. Aziz *et al.* (EHS-RCBC Collaboration), Z. Phys. C **30**, 381 (1986).

[6] M. Y. Bogolyubsky *et al.*, Yad. Fiz. **50**, 683 (1989) [Sov. J. Nucl. Phys. **50**, 424 (1989)].

[7] M. Aguilar-Benitez *et al.*, Z. Phys. C **50**, 405 (1991).

[8] K. Böckmann *et al.* (Bonn-Hamburg-Munich Collaboration, Aachen-Bonn-CERN-Cracow Collaboration), Nucl. Phys. B **166**, 284 (1980).

[9] M. Abdel-Bary *et al.* (COSY-TOF Collaboration), Eur. Phys. J. A **46**, 27 (2010).

[10] M. Abdel-Bary *et al.* (COSY-TOF Collaboration), Eur. Phys. J. A **48**, 37 (2012).

[11] G. Agakishiev *et al.* (HADES Collaboration), Eur. Phys. J. A **49**, 34 (2013).

[12] G. Agakishiev *et al.* (HADES Collaboration), Phys. Rev. C **90**, 015202 (2014).

[13] G. Agakishiev *et al.* (HADES Collaboration), Phys. Rev. C **85**, 035203 (2012).

[14] G. Agakishiev *et al.* (HADES Collaboration), Nucl. Phys. A **881**, 178 (2012).

[15] G. Agakishiev *et al.* (HADES Collaboration), Phys. Rev. C **87**, 025201 (2013).

[16] G. Agakishiev *et al.* (HADES Collaboration), Phys. Lett. B **742**, 242 (2015).

[17] G. Agakishiev *et al.* (HADES Collaboration), Eur. Phys. J. A **41**, 243 (2009).

[18] K. Olive *et al.* (Particle Data Group), Chin. Phys. C **38**, 090001 (2014).

[19] I. Fröhlich *et al.*, PoS **ACAT2007**, 076 (2007).

[20] G. Agakishiev *et al.* (HADES Collaboration), Eur. Phys. J. A **48**, 64 (2012).

[21] J. Reed, A. Melissinos, N. Reay, T. Yamanouchi, E. Sacharidis, *et al.*, Phys. Rev. **168**, 1495 (1968).

[22] J. F. Donoghue, Phys. Rev. D **17**, 2922 (1978).